Research in Astron. Astrophys. **2011** Vol. **11** No. **1**, 63–70
http://www.raa-journal.org *http://www.iop.org/journals/raa*

Research in Astronomy and Astrophysics

1_{10}–1_{11} H_2CO and $H_{110\alpha}$ observations towards the giant HII region in cloud complex W43 *

Gang Wu[1,2], Jarken Esimbek[1], Jian-Jun Zhou[1] and Xiao-Hong Han[1,2]

[1] National Astronomical Observatories / Urumqi Observatory, Chinese Academy of Sciences, Urumqi 830011, China; *wug@uao.ac.cn*
[2] Graduate University of Chinese Academy of Sciences, Beijing 100049, China

Received 2010 May 10; accepted 2010 July 7

Abstract The 1_{10}–1_{11} formaldehyde (H_2CO) absorption line and $H_{110\alpha}$ radio recombination line (H RRL) are observed towards the giant HII region in cloud complex W43. The observations are obtained using the Nanshan 25 m single dish operated by Urumqi Observatory, National Astronomical Observatories of China. A region about $30' \times 30'$ is observed, which covers the whole HII region in W43. Except for the central $10'$ region, all the other seven points are first observed with the H_2CO 1_{10}–1_{11} absorption. The column density of the H_2CO is calculated, and the H_2CO density contours show some differences with the infrared image. Multiple features appear in the H_2CO and H RRL which indicate complex structure. The intensities of the H_2CO and the velocities of the $H_{110\alpha}$ seem to present a linear correlation, which illustrates that the sphere of influence of the central WR/OB cluster may be much more extended than presently known, since the size is nearly 50 pc.

Key words: ISM: radio lines — HII regions — stars: formation

1 INTRODUCTION

The 6 cm (1_{10}–1_{11}) H_2CO absorption line was first detected in 1969 (Snyder et al. 1969). Then in the same year, Palmer et al. (1969) reported that they detected anomalous absorption in the direction of four dark nebulae. To achieve such a low exciting temperature, there must be a non-thermal cooling mechanism, thus the pumping mechanism which produces the excess of the lower state was proposed by Townes & Cheung (1969), through an idealized classical calculation, giving a reasonable explanation: by collisions with the neutral particles, the exciting temperature of the 1_{10}–1_{11} transition of H_2CO could be below 2.7 K. Evans et al. (1975) scrutinized various models through the 2 cm (2_{11}–2_{12}) observations, and confirmed that the collisional pumping model had the best agreement with the observations. Owing to the extremely low exciting temperature and relatively low density, H_2CO is commonly considered to be a good probe of low temperatures and dense nebulae. In addition, the survey of Downes et al. (1980) demonstrated that 80% of the HII region was associated with the H_2CO, and so H_2CO is an important tracer of star formation regions. Therefore, we can acquire information about reactions between the newly formed stars and the surrounding gas.

* Supported by the National Natural Science Foundation of China.

W43 is well known for its extended HII region (which is excited by a star cluster). The distance to W43 is listed in several descriptions, and in recent works it is believed to be about 5.5–6 kpc away (Wilson et al. 1970; Bania et al. 1997; Balser et al. 2001). Near-infrared images revealed a dense stellar cluster in its center, where three stars are identified. One is a Wolf-Rayet star of subtype WN7, and the other two are O-type giants or supergiants (Blum et al. 1999). W43 has been mapped with CO lines and several continuum observations, parts of which have HCO^+, ^{13}CO (Motte et al. 2003; Bieging et al. 1982; Subrahmanyan & Goss 1996; Goss & Shaver 1970; Liszt 1995) and H_2CO absorptions. However, according to our knowledge, there are few H_2CO mapping studies of W43 (Fomalont & Weliachew 1973; Bieging et al. 1982; Martín-Pintado et al. 1985). Moreover, all the previous observations are limited to a small region (about 10 arcmin). Thus, relatively extended H_2CO observations are lacking. Another important problem in the understanding of W43 involves the giant HII region, which is the sphere of influence of the WR/OB cluster. Motte et al. (2003) claimed that it remains unclear if this first episode of star formation is triggering the formation of new massive stars and they also verified that at least two of the three IRAS point sources are possibly excited by the nearby WR/OB cluster. Because the H RRL is a unique tool to trace the HII region, W43 is also observed with the H RRL in order to make a comparison. A comparison of MSX (Midcourse Space Experiment) infrared data at A-band is also carried out. The MSX was launched on 1996 April 24 and surveyed the whole Galactic plane at A(8.28 μm), B_1(4.29 μm), B_2(4.35 μm), D(14.65 μm) and E(21.34 μm). The infrared data in the A-bank are obtained to understand the relationship with our observations. Subsequently, the continuum observations are obtained to calculate the parameters.

The parameters of the telescope are listed in the following section, then the results and discussion of the observations are described in Section 3. Finally, the conclusions are summarized in Section 4.

2 OBSERVATIONS

Single-dish observations were made from 2008 September to 2010 January with the Nanshan 25 m radio telescope operated by Urumqi Observatory, National Astronomical Observatories of China. Our observations were centered at 4851.9102 MHz with a bandwidth of 80 MHz , which simultaneously covered the H RRL at 4874.1570 MHz and the H_2CO absorption line at 4829.6594 MHz. At this frequency, the half power width of the main beam was about 10 arcmin. A digital autocorrelation spectrometer with 4096 channels was used, which means the velocity resolution was 1.206 km s^{-1}, affording an 80 MHz bandwidth. The pointing and tracking accuracy was better than 20 arcseconds, and the beam efficiency was 0.65. The system temperature was about 23 K. The DPFU (Degrees Per Flux Unit) value was 0.116 K Jy^{-1}.

The so-called on-off model was used in the observations, with 6 min integrations in the off position, then the same integration time was used on the source. If the S/N did not achieve the expected value, the on-off observational cycle would be repeated. The total integration time at each point ranged from 30 min to several hours. A diode noise source was used to calibrate the spectrum and the flux error was 15%. Continuum intensity was derived from the baseline of the spectra.

3 RESULTS AND DISCUSSION

Nine points were observed towards W43, covering an area of about $30' \times 30'$. The observations were centered at the the point (0, 0), which corresponds to α =$18^h47^m36.04^s$, δ = –15638.9. The 6 cm absorption line was detected in eight of the nine observed points. Except for the point (0, 0), all the other seven points were first observed with the 6 cm H_2CO absorption line. In addition, H RRL could also be detected in eight points. These two lines in a non-detected point may be too weak to be identified. The signal to noise ratio of all the detected points was better than 3. The GILDAS package was used in data processing, and all of the parameters obtained are summarized in Table 1. Cols. (1) and (2) indicate the equatorial coordinates, the offset is given in Col. (3), and Col. (4) shows

the total integration time of each point. The $V_{\rm lsr}$, line width, and the intensity and column density of H_2CO are, respectively, given in Cols. (5)–(8). Moreover, observational parameters of H RRL ($V_{\rm lsr}$, line width, and intensity) are listed in Cols. (9)–(11). The data in the last column are the continuum intensities.

Table 1 Observed and Derived Parameters

				H_2CO				$H_{110\alpha}$			T_c
α	δ	offset	$T_{\rm int}$	$V_{\rm lsr}$	δv	Intensity	Column density	$V_{\rm lsr}$	δv	Intensity	
(J2000)	(J2000)	(arcmin)	(min)	(km s^{-1})		(Jy)	(cm^{-2})	(km s^{-1})		(Jy)	(K)
(1)	(2)	(3)	(4)	(5)	(6)	(7)	(8)	(9)	(10)	(11)	(12)
18 48 16.06	−02 06 38.9	1, −1	30			< 0.4				< 0.4	
18 47 36.04	−02 06 38.9	0, −1	60	91.750	6.618	1.8096	9.3637E+12	56.061	43.254	0.1664	
								96.826	30.851	0.4656	12.8412
18 46 56.01	−02 06 38.9	−1, −1	260	87.685	6.170	0.4598		44.899	29.993	0.1522	
				93.271	4.445	0.9241	1.8068E+12	98.886	38.309	0.1547	11.3079
18 46 56.01	−01 56 38.9	−1, 0	108	91.719	5.976	2.2004	10.7717E+12	44.571	37.880	0.1679	12.1839
								96.008	38.051	0.2829	
18 47 36.04	−01 56 38.9	0, 0	102	7.889	2.563	0.3459		56.111	52.971	0.3009	78.7580
				12.824	3.092	0.7748		93.351	29.144	1.4560	
				81.805	4.497	1.4091					
				92.498	6.990	5.8177	5.5362E+12				
18 48 16.06	−01 56 38.9	1, 0	120	94.288	7.338	0.7477		56.980	36.650	0.1150	14.4068
				101.717	4.990	0.3007	3.8722E+12	100.385	29.426	0.3321	
18 48 16.06	−01 46 38.9	1, 1	378	77.333	4.379	0.3008		48.419	32.961	7.0532E–02	8.7346
				82.190	4.631	0.1102		101.888	32.265	0.2355	
				92.077	3.177	0.2585					
				100.937	1.683	0.1620					
				104.942	3.588	0.1579	9.1850E+11				
18 47 36.04	−01 46 38.9	0, 1	60	75.499	4.419	0.7001		45.753	38.300	0.1085	15.9568
				84.109	4.076	0.3267		97.654	28.931	0.3420	
				95.385	8.314	1.1060	5.8907E+12				
18 46 56.02	−01 46 38.9	−1, 1	300	61.103	2.947	0.3546		39.506	24.168	0.1589	9.3211
				74.793	3.049	0.4264		96.188	42.113	0.1305	
				83.571	5.998	0.5318					
				96.279	6.491	1.7332	11.7712E+12				

As we can see in the observed spectra of Figure 1, several velocity features appear in all the detected spectra. An intense feature at velocities 91–96 km s^{-1} appeared in all detected points. Gaussian fittings have been performed, and the results are tabulated in Table 1. The intensity of the feature at 92.498 km s^{-1} in the point (0, 0) is much stronger than the corresponding feature in the other points.

Bieging et al. (1982) claimed that they observed two additional H_2CO absorption features in the velocity range 5–17 km s^{-1}. In our observations, these features also appeared in the point (0, 0) (Fig. 2). Four features are detected in this region, and their velocities are 7.889, 12.824, 81.805 and 92.498 km s^{-1} respectively. Figure 3 shows the spectra of the H RRL toward W43. An interesting characteristic can be seen in the H RRL observations. In every detected point, there are two velocity features (Fig. 3). A Gaussian fitting is also performed (parameters are also listed in Table 1). The contours of the two H RLL features (top two panels), the column density (left bottom panel) and the intensity (right bottom panel) of H_2CO are all drawn in Figure 4.

According to Bieging's advice, the antenna temperature maps of the H_2CO absorption line are strongly biased by the continuum emission (Bieging et al. 1982). Therefore, the antenna temperature may not precisely exhibit the distribution of the H_2CO. Thus, a contour of column density is made in this paper, and relevant equations are listed as follows. We can obtain the formula directly from the equation of radiative transfer,

$$\tau_{\rm app} = -\ln\left[1 - \frac{T_L}{T_{\rm c} + T_{\rm b} - T_{\rm ex}}\right], \quad (1)$$

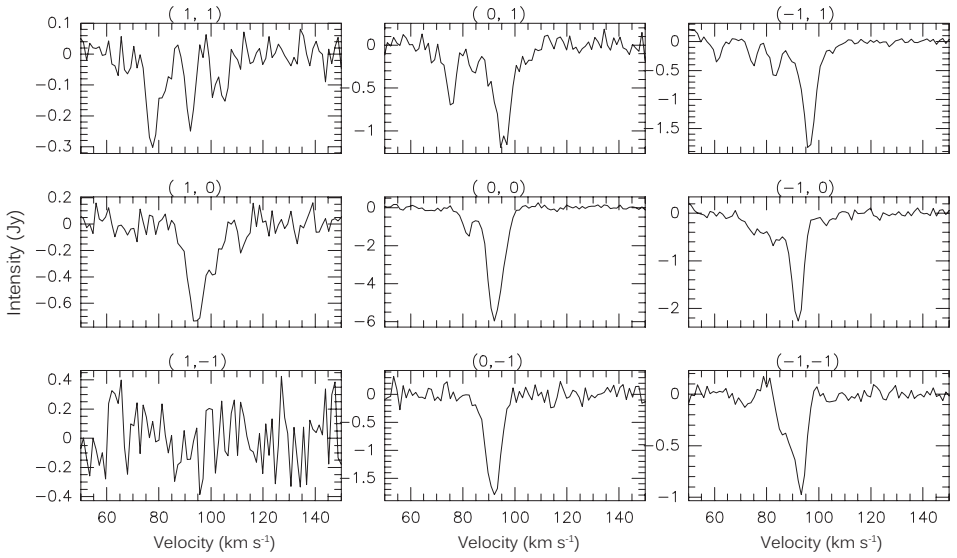

Fig. 1 A mosaic of the H_2CO absorption lines observed in W43. The S/N ratios of the detected spectra are all better than 3. The number on the box is the offset of each point. The (0,0) point corresponds to $\alpha = 18^{\rm h}47^{\rm m}36.04^{\rm s}$, $\delta = -1^\circ 56' 38.9''$.

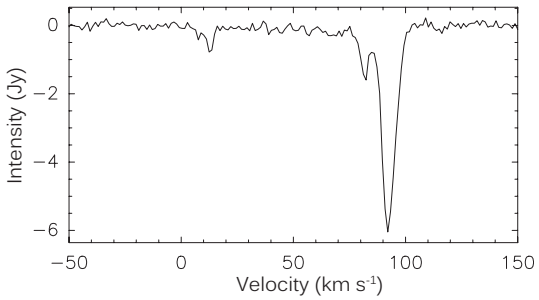

Fig. 2 H_2CO absorption features at the point $(0, 0)$. Four absorption lines appeared in this region. Their velocities are 7.889, 12.824, 81.805 and 92.498 km s^{-1} respectively.

where T_L is the measured brightness temperature and $T_{\rm c}$ is the continuum intensity, which is obtained directly from our observations. Cosmic background temperature $T_{\rm b}$ is set to 2.7 K. $T_{\rm ex}$ is the exciting temperature of the state 1_{10}–1_{11}, which is assumed to have a characteristic value 1.7 K (Garrison et al. 1975).

Then, the column density of H_2CO is calculated from

$$N_{\rm H_2CO} = 9.4 \times 10^{13} \tau_{\rm app} \Delta V \,, \tag{2}$$

where $\tau_{\rm app}$ is the apparent optical depth calculated in Equation (1), and ΔV is the line width of the H_2CO absorption line. The calculated column densities are displayed in Table 1. Also, we drew a contour plot of the column density (the bottom-left panel in Fig. 4). The contours of integrated intensity of the H_2CO absorption are also sketched (the bottom-right one). The two panels are all overlaid on the infrared image at A-band of the MSX.

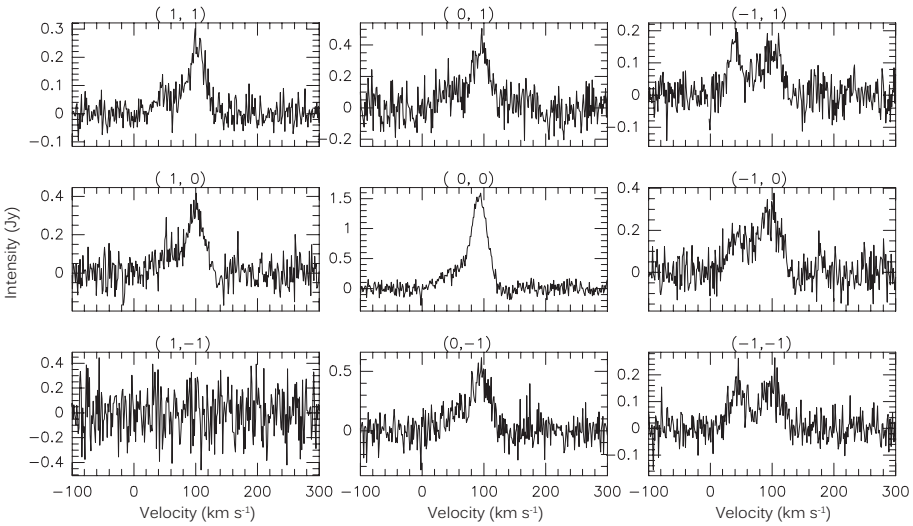

Fig. 3 A mosaic of the H RRLs observed in W43. The S/N ratios of the detected spectra are all better than 3. The number on every box is the offset. The (0, 0) point corresponds to $\alpha = 18^{\rm h}47^{\rm m}36.04^{\rm s}$, $\delta = -1^\circ 56' 38.9''$.

As we can see in the bottom two panels in Figure 4, the peaks of the left contour and the infrared image are all located at the center point (0, 0), but the contour of the H_2CO density (right panel) shows two peaks which are located to the south and the north-west of the point (0, 0), respectively. Moreover, in the left panel, no absorption line is detected to the south-east of the point (0, 0), but a relatively strong infrared characteristic is shown. The north-west of point (0, 0) shows the opposite phenomenon. A relatively strong H_2CO absorption feature is detected in the weak infrared region. So, the contours of the integrated intensity exhibit rough association with the infrared image, but there are also some differences. The reason that the peak of the integrated intensity does not coincide with the peak of the density contour can be explained by Equation (1), where T_L is dominated by both $\tau_{\rm app}$ and $T_{\rm c}$. Because the background radiation in the center is much stronger, even with a relatively small density, T_L may also be intense. The density of the H_2CO is small in the center and increases away from the (0, 0) point, and shows two peaks beside the point (0, 0). The contours of the density of the H_2CO seem not to show much more association with the infrared image. A probable reason is the relatively lower dissociation energy of the formaldehyde, and the formaldehyde is more easily photodissociated near the photon-dominated regions (Rodríguez et al. 2007). The UV emission from the WR/OB cluster is much stronger in the center, which means the formaldehyde in the center is more likely to be photodissociated, therefore the density of the formaldehyde in the center is relatively small and the density in the region beside the center will be relatively larger.

From Figure 1, we can see that multiple lines are exhibited at every point. That means there must be several velocity components in one beam. Liszt (1995) has verified that there are many shells or loops with different velocities in W43. Thus, the velocity components may come from these shells. In Figure 2, we have shown that there are two additional features with velocity 7.889 and 12.824 km s^{-1} observed at the point (0, 0). Bieging et al. (1982) also detected these components; moreover their explanation was that a separated dark cloud is located even closer to the Sun, and the calculated kinematic distance is about 1 kpc. We detected these features only at the point (0, 0). In addition, the background radiation in non-detected points is not very weak. So, the components with velocity 7.889 and 12.824 km s^{-1} in the non-detected region are very thin or the sizes of these components

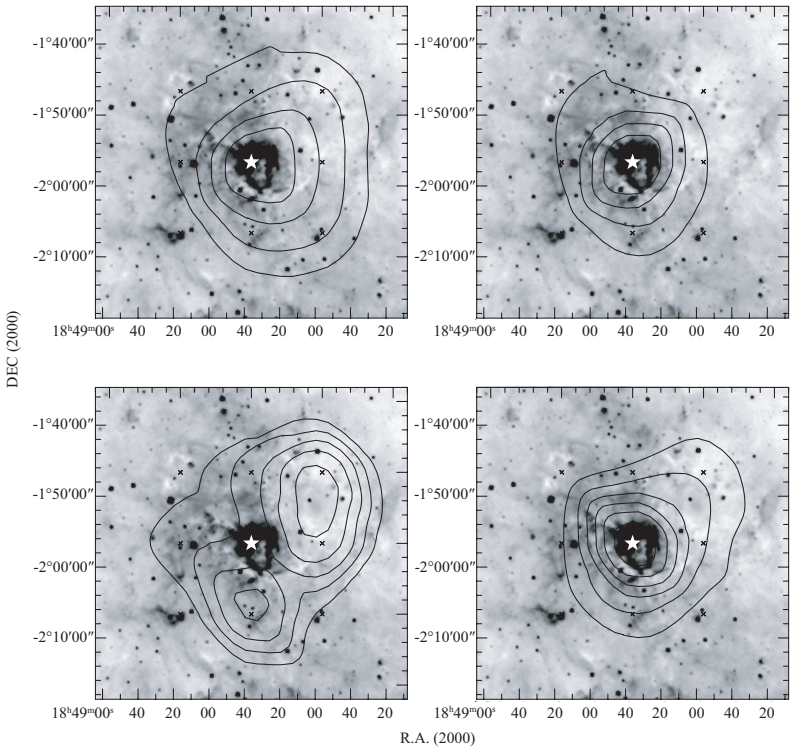

Fig. 4 Contours of the observations of W43. All the contours are sketched in the MSX 8μm image. The top two panels are contours of the two H RRL features, the left one corresponds to the feature at velocity 39–56 km s^{-1}; the right one depicts the feature at velocity 93–101 km s^{-1}. The bottom-left panel shows the contours of the H_2CO column density. The bottom-right one shows the distribution of the integrated intensity of the H_2CO absorption feature in the velocity range 91–96 km s^{-1}. The marked star illustrates the center point (0, 0) which corresponds to α = $18^{\rm h}47^{\rm m}36.04^{\rm s}$, δ = –1°56′ 38.9″. The observed points are shown as $\times$ symbols in all the images.

are limited to only be within 10′. As has been mentioned in the results, double features existed in all of the H RRL observations. The features in the velocity range 39–56 km s^{-1} are always accompanied by the features in the velocity range 93–101 km s^{-1}. Two contours are also drawn which correspond to these two features on the MSX infrared image at A band (top two panels in Fig. 4). As we can see in Figure 4, in these images, the peaks of the two contours coincide. We can see the intensities of the two velocity features in Table 1, as well as the positions of peak intensity, are all located at the point (0, 0). However, the intensities of the two features seem not to be correlated. In order to show this more directly, Figure 5 is drawn to show the comparison between the intensities at the same point. We reject the (0, 0) point because its overwhelming intensity biases the differences with the other points. As we can see in Figure 5, the two features are not associated with each other very much. Therefore, the two features in each point seem not to come from one HII region. So, it is reasonable to say that these two features seem to overlap but come from different HII regions. In this study, that means in each direction, there are always two accompanying HII regions.

We found that the intensities of the strong H_2CO feature (at 91–96 km s^{-1}) and the velocities of the strong H RRL feature (at 93–101 km s^{-1}) seem to present a linear relationship. Figure 6 shows the relationship between the two parameters. All the data are sketched in the left panel. The right

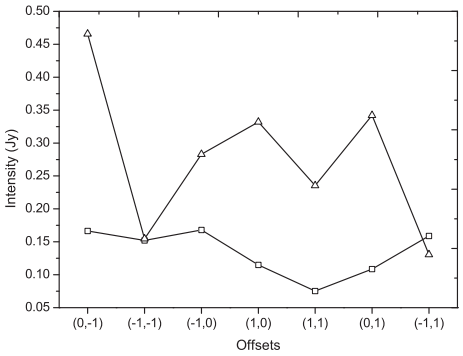

Fig. 5 Comparison of the intensities of the two $H_{110\alpha}$ features at each point excluding the (0, 0) point. The numbers labeled below the x-axis denote offsets and the y-axis indicates the intensity of the H RRL.

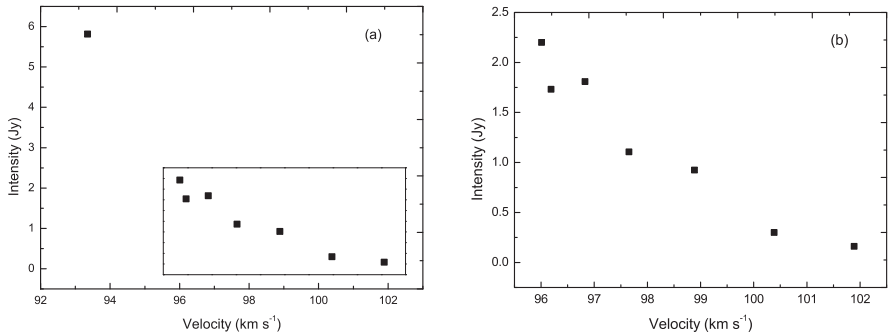

Fig. 6 Velocities of the H RRL vs. intensities of the H_2CO absorption line. (a) all the detected data are sketched on this panel; (b) Magnification of the square region in the left panel.

one is a magnification of the square region in the left panel which excludes the (0, 0) point. Also, we can clearly see that as the velocity increases, the intensity of the H_2CO line decreases. A linear fit of the right panel is made.

$$I_{\mathrm{H_2CO}} = 29.978 - 0.292 V_{\mathrm{H_{110\alpha}}} \, . \tag{3}$$

Although the explanation of this linearity is lacking, we can still make an inference using this relationship. From the bottom-right panel of Figure 4, we can see that $I_{\mathrm{H_2CO}}$ decreases as we move farther from the point (0, 0). In addition, the $V_{\mathrm{H_{110\alpha}}}$ increases as we move away from the peak position, which will fulfil the condition that $I_{\mathrm{H_2CO}}$ varies inversely with the $V_{\mathrm{H_{110\alpha}}}$. Here we present a hypothesis: assume that in the center there is a triggered source (WR/OB cluster) behind, and it drives an arc ionization moving towards us, then when the position from (0, 0) increases, the angle between the direction of arc motion and the line of sight becomes larger. The projection of the velocity along the line of sight will decrease. The $V_{\mathrm{H_{110\alpha}}}$ equals the W43 systematic velocity minus the projection of the arc velocity. So when the distance from the (0, 0) point is larger, the $V_{\mathrm{H_{110\alpha}}}$ will increase. Therefore, this relationship may illustrate that all the star formation within the size we observe is triggered by the WR/OB cluster. Motte et al. (2003) have claimed the HII region excited by the W43 starburst cluster would cover up to 13 pc. However, according to our observations, the size may be nearly 50 pc assuming that the distance is 5.5 kpc.

4 CONCLUSIONS

The conclusions can be summarized in three points.

First, relatively extended mapping observations of W43 were made using the 25 m antenna. Seven points of W43 were observed with the H_2CO absorption line for the first time, with the exception of point (0, 0). The column densities are calculated and a contour of the H_2CO distribution is obtained. By comparing with the infrared image, the contours of the integrated intensity exhibit some association with the infrared image, but there are also some differences; however, the contour of the density of the H_2CO seems not to show much more association with the infrared image. The reason may be because the formaldehyde is easily photodissociated near the photon-dominated regions. (Rodríguez et al. 2007). More formaldehyde is dissociated in the center where the UV emission from the WR/OB cluster is much stronger, so the density in the center is relatively small and the region away from the center may show a larger density.

Second, multiple features are excited in both the H_2CO and $H_{110\alpha}$, illustrating a complicated structure. So, high resolution telescope or even synthesized telescope observations could be taken. Two other features of the H_2CO absorption with velocities 7.889 and 12.824 km s^{-1} were only detected in the point (0, 0); we suppose that the size of this component is limited to be in $10'$. Double features appeared in all the radio observations. Contours of the two components are made. Although the peaks match, we think that they come from different HII regions of W43.

Finally, the intensities of the H_2CO and the velocities of the $H_{110\alpha}$ seem to present a linear correlation. We hypothesize that a triggered source, like a WR/OB cluster, lies behind from our perspective and excites an arc ionization front, which would explain the observations. Our observations show that the sphere of influence of the central WR/OB cluster is much more extended than previously believed. Within the approximately 50 pc region we observed, star formation is triggered by the cluster.

Acknowledgements This work is supported by the National Natural Science Foundation of China (Grant Nos. 10778703, 10873025) and the Program of Light in China's Western Region (LCWR, Nos. RCPY200605, RCPY200706).

References

Balser, D. S., Goss, W. M., & De Pree, C. G. 2001, AJ, 121, 371
Bania, T. M., Balser, D. S., Rood, R. T., Wilson, T. L., & Wilson, T. J. 1997, ApJS, 113, 353
Bieging, J. H., Wilson, T. L., & Downes, D. 1982, A&AS, 49, 607
Blum, R. D., Damineli, A., & Conti, P. S. 1999, AJ, 117, 1392
Downes, D., Wilson, T. L., Bieging, J., & Wink, J. 1980, A&AS, 40, 379
Evans, N. J., II, Zuckerman, B., Morris, G., & Sato, T. 1975, ApJ, 196, 433
Fomalont, E. B., & Weliachew, L. 1973, ApJ, 181, 781
Garrison, B. J., Lester, W. A., Jr., Miller, W. H., & Green, S. 1975, ApJ, 200, L175
Goss, W. N., & Shaver, P. A. 1970, Australian Journal of Physics Astrophysical Supplement, 14, 1
Liszt, H. S. 1995, AJ, 109, 1204
Martín-Pintado, J., Wilson, T. L., Gardner, F. F., & Henkel, C. 1985, A&A, 142, 131
Motte, F., Schilke, P., & Lis, D. C. 2003, ApJ, 582, 277
Palmer, P., Zuckerman, B., Buhl, D., & Snyder, L. E. 1969, ApJ, 156, L147
Rodríguez, M. I., Wiklind, T., Allen, R. J., Escalante, V., & Loinard, L. 2007, ApJ, 633, 824
Snyder, L. E., Buhl, D., Zuckerman, B., & Palmer, P. 1969, Phys. Rev. Lett., 22, 679
Subrahmanyan, R., & Goss, W. M. 1996, MNRAS, 281, 239
Townes, C. H., & Cheung, A. C. 1969, ApJ, 157, 103
Wilson, T. L., Mezger, P. G., Gardner, F. F., & Milne, D. K. 1970, A&A, 6, 364